Published in final edited form as:
Nature. 2015 August 13; 524(7564): 239–242. doi:10.1038/nature14568.

Live imaging RNAi screen reveals genes essential for meiosis in mammalian oocytes

Sybille Pfender[#], **Vitaliy Kuznetsov**[#], **Michał Pasternak**[#], **Thomas Tischer**, **Balaji Santhanam**, and **Melina Schuh**[1]

Medical Research Council, Laboratory of Molecular Biology, Francis Crick Avenue, Cambridge Biomedical Campus, Cambridge CB2 0QH, United Kingdom

[#] These authors contributed equally to this work.

Abstract

During fertilization, an egg and a sperm fuse to form a new embryo. Eggs develop from oocytes in a process called meiosis. Meiosis in human oocytes is highly error-prone[1,2], and defective eggs are the leading cause of pregnancy loss and several genetic disorders such as Down's syndrome[3-5]. Which genes safeguard accurate progression through meiosis is largely unclear. Here, we developed high-content phenotypic screening methods for the systematic identification of mammalian meiotic genes. We targeted 774 genes by RNAi within follicle-enclosed mouse oocytes to block protein expression from an early stage of oocyte development onwards. We then analysed the function of several genes simultaneously by high-resolution imaging of chromosomes and microtubules in live oocytes and scored each oocyte quantitatively for 50 phenotypes, generating a comprehensive resource of meiotic gene function. The screen generated an unprecedented annotated dataset of meiotic progression in 2,241 mammalian oocytes, which allowed us to analyse systematically which defects are linked to abnormal chromosome segregation during meiosis, identifying progression into anaphase with misaligned chromosomes as well as defects in spindle organization as risk factors. This study demonstrates how high-content screens can be performed in oocytes, and now allows systematic studies of meiosis in mammals.

[1]**Corresponding author** Correspondence to: Melina Schuh (mschuh@mrc-lmb.cam.ac.uk) .

Contributions

All authors analysed data. S.P. microinjected the majority of siRNA mixes, and identified, validated and characterised most genes; M.P. microinjected siRNA mixes, compared the developmental capacity and expression profile of *in vitro* and *in vivo* grown oocytes, and identified, validated and characterised several genes; V.K. microinjected siRNA mixes and wrote software in OriginPro to quantify phenotypes; T.T. validated and characterised *Dusp7*; B.S. did all bioinformatics analyses; V.K. and M.S. developed and established the strategy of the screen; M.S. wrote the manuscript; S.P., M.P., T.T. and B.S. commented on and edited the manuscript; M.P. and M.S. prepared the revised manuscript; M.S. supervised the study.

Supplementary Information is linked to the online version of the paper at www.nature.com/nature.

Data deposition

RNA-Seq data have been submitted to NCBI GEO under the accession number GSE68150.

Competing financial interests

The authors declare no competing financial interests.

Europe PMC Funders Author Manuscripts

Meiosis is still much more poorly understood than mitosis, especially in mammals. Systematic screens have greatly increased our understanding of mitosis. However, high-content screens for mammalian meiotic genes have so far been precluded by various technical challenges. For instance, mammalian oocytes are only available in small numbers; genetic screens in mammals are slow; and RNAi in oocytes is inefficient due to large amounts of stored protein. Oocytes accumulate proteins while they grow within follicles in the ovary[6]. Thus, we established a protocol that allowed us to block protein expression by RNAi during follicle growth and to subsequently assess gene function by quantitative live imaging (Fig. 1a). Briefly, we microinjected siRNAs into small follicle-enclosed oocytes and grew the follicles *in vitro*, combining and modifying previous methods[7-9]. When the oocytes had reached their full size, we isolated and labelled them, and imaged meiosis live for around 18 h on confocal microscopes using automated imaging routines.

The *in vitro* grown oocytes resembled *in vivo* grown oocytes: firstly, the efficiency of nuclear envelope breakdown (NEBD) and polar body extrusion, as well as the timing of meiotic progression were similar (Fig. 1b-d; Extended Data Fig. 1d, e); secondly, their transcriptome was related (Extended Data Fig. 2a-c; Supplementary Table 1); thirdly, they developed into blastocysts with similar efficiency upon fertilisation (Extended Data Fig. 1f, g)[8].

Follicle culture and microinjection are labour-intensive, precluding genome-wide screens. Instead, we preselected 774 target genes that were highly expressed in mouse oocytes, while excluding mRNAs stored for embryo development. To this end, we took advantage of two microarray data sets[10,11], which compare the expression profile of oocytes with the profiles of other cell types and preimplantation mouse embryos, respectively (Fig. 1f). Only genes that were significantly upregulated in oocytes in both data sets were selected for the screen.

To achieve high-throughput, we targeted twelve genes simultaneously (Fig. 1a, e). Co-depletion of several genes led to the expected phenotype for genes with known functions. For instance, mixes targeting one of the zona pellucida genes (*Zp1*, *Zp2*, or *Zp3*) together with 11 other genes prevented formation of the zona[12] (Extended Data Fig. 1h, i), and mixes targeting spindle assembly checkpoint proteins led to the expected earlier onset of anaphase (e.g. Mix 33P1-2-3-4-5-6 targeting *Bub1* in Supplementary Table 2).

The targeting of all 774 genes resulted in videos of 2,241 individual oocytes, including 1,210 RNAi-treated and 1,031 control oocytes. We scored every oocyte for 41 possible defects and determined 5 characteristic meiotic time points as well as the spindle length and width in meiosis I and II (Supplementary Table 3; Scored parameters are described in Extended Data Fig. 3). The frequencies with which different defects were observed in RNAi-treated and control oocytes are plotted in Fig. 2 and Extended Data Figs. 4a-i and 5. To identify significant hits, we calculated the Z-score of individual mixes for different categories. These quantifications resulted in a comprehensive annotated resource of defects (Supplementary Tables 2 and 3; Extended Data Fig. 2d). Supplementary Table 2 allows users to easily query if siRNA mixes targeting their gene of interest resulted in defects in oocyte meiosis or to identify mixes causing defects in the stage of meiosis that they are

studying. This table also includes hyperlinks to the original video files for further assessment.

Proof-of-principle experiments demonstrated that defects observed upon targeting several genes simultaneously could be allocated to individual genes by stepwise splitting of siRNAs into smaller pools (Fig. 1g; Extended Data Fig. 4j). Several of the identified genes have not yet been implicated in mouse oocyte meiosis, demonstrating that this screening strategy is suitable to identify new meiotic genes. Hits were verified typically three times when the siRNA mixes were split to track down the genes that caused the phenotype of interest. To confirm the observed defects, siRNAs were microinjected again upon gene identification. In addition, specificity was confirmed by microinjection of individual siRNAs and rescue experiments as detailed below.

The screen identified several genes that control meiotic progression, including *Dusp7*, a poorly characterized dual-specificity phosphatase. More than 40% of *Dusp7*-depleted oocytes failed to undergo NEBD (Fig. 3a, b; Supplementary Video 1). In the remaining 60%, NEBD was significantly delayed (Fig. 3c). NEBD could be rescued by wildtype EGFP-DUSP7, but not by the catalytically inactive EGFP-DUSP7 C333S mutant (Fig. 3b), indicating that DUSP7's phosphatase activity is essential for NEBD. EGFP-DUSP7 was excluded from the nucleus (Fig. 3d), suggesting that it promotes NEBD by dephosphorylating cytoplasmic proteins. Together, these data identify *Dusp7* as a phosphatase essential for NEBD in oocytes.

Also *Eif4enif1* was essential for meiotic progression. Mutations in *Eif4enif1* have recently been detected in a family with premature ovarian failure[13]. The mechanism by which *Eif4enif1* affects fertility is unclear. Our results show that *Eif4enif1* is essential for NEBD and resumption of meiosis (Extended Data Fig. 6a, b).

The screen also provided insights into causes of chromosome segregation errors in oocytes. Several genes were essential for accurate chromosome segregation, including the uncharacterized genes *Fam46b* and *Fam46c* (family with sequence similarity 46), *Aspm*[14] (Extended Data Fig. 7 and Supplementary Video 2), *Birc5* (Survivin)[15] (Extended Data Figs. 6), *Ttk*[16] and *Mastl* (Fig. 3e, g). MASTL was also required to prevent exit from meiosis after anaphase I (Fig. 3e, f), but dispensable for meiotic resumption, progression into anaphase, chromosome condensation or cytokinesis (Fig. 3h, i; Extended Data Fig. 8), consistent with a recent study[17].

The screen also allowed us to analyse on a global level how chromosome segregation errors arise in oocytes. With data from 2,241 oocytes, it generated the largest existing data set of meiosis in mammalian oocytes (Supplementary Table 2). Evaluation of the control data set identified progression into anaphase with misaligned chromosomes as major contributor to chromosome segregation errors: misaligned chromosomes only delayed but did not prevent progression into anaphase (Fig. 4a, b). This is consistent with the model that the spindle assembly checkpoint in mammalian oocytes is less stringent than in mitosis[4,5].

We were also able to analyse systematically which defects in the oocyte precede chromosomes that lag behind during anaphase. This is of particular interest because lagging

chromosomes can lead to inappropriate partitioning of chromosomes upon cytokinesis and are a major cause of aneuploidy[18,19]. We identified chromosome alignment, individualization and stretching as well as spindle defects as risk factors (Fig. 4c). A systematic representation of how different defects in oocytes were linked is shown in Extended Data Figs. 9 and 10.

In summary, we have established an experimental system that now allows systematic studies of meiosis in mammals. The screening approach is scalable and could also be adapted to investigate fertilization or embryo development. The follicle-based RNAi method will also be a powerful tool for individual gene studies, as it allows proteins with low turnover to be depleted in oocytes and preimplantation embryos. The techniques presented in this study should thus facilitate a more rapid build-up of knowledge about meiosis and early embryo development in mammals, which is crucial to improve methods for treating fertility problems in humans.

METHODS

Preparation, microinjection and culture of follicles

All mice were maintained in a specific pathogen-free environment according to UK Home Office regulations. Ovaries were dissected from two to five 10-12 day old (C57BL × CBA) F1 females. To obtain individual follicles, the ovaries were incubated in modified MEM-alpha medium optimized for *in vitro* culture of follicles (MEM-alpha (Gibco 12000-014) supplemented with 0.026M $NaHCO_3$ (Sigma), 5678U/100 ml Penicillin G (Sigma) and 8265U/100ml Streptomycin (Sigma), 1x ITS (Insulin/Transferrin/Selenium Solution; Sigma; Stock is 100x), 5% FBS (Fetal Bovine Serum; Gibco 16000044) and 0.01 μg/ml FSH (Follicle Stimulating Hormone; National Hormone and Peptide Program, NDDK-oFSH-20) that was supplemented with 2 mg/ml collagenase (Roche) for about 30-40 minutes total. During incubation with collagenase, the ovaries were pipetted up and down every 10 minutes to facilitate dissociation and then washed through several droplets of follicle culture medium without collagenase. The follicles where then randomly allocated into control siRNA and RNAi mix injection groups. Intact follicles were then loaded into a microinjection chamber prepared with two double stick tapes as spacer and microinjected as previously described[7] in culture medium supplemented with HEPES (Sigma). Upon microinjection, they were cultured at 37°C in 5% CO_2 on membrane inserts in 6 well or 12 well culture dishes filled with follicle culture medium (see above). For most experiments, collagen-coated inserts from Corning were used (Transwell® COL), but also Transwell-Clear inserts that were coated with 10 μg/cm^2 collagen solution Type I from rat tail (Sigma), BD Matrigel™ Basement Membrane (BD Biosciences; thin coating method) as well as BD BioCoat™ filters were successfully used (Extended Data Fig. 1c). Medium surrounding the filter was replaced with fresh medium every 3-4 days. Oocytes were isolated from follicles after 10-11 days of *in vitro* culture. To this end, the oocytes were stripped with a small glass pipette and released into modified M2 medium that contained 10% FBS instead of BSA as well as 100 ng/ml FSH and dbcAMP. Oocytes were subsequently microinjected with mRNAs encoding mEGFP-α-tubulin (spindle) and H2B-mRFP (chromosomes). Upon microinjection, oocytes were cultured for up to 3.5 hours at 37°C until fluorescent proteins

were expressed. Oocytes were then released from prophase arrest by transferring them into medium without dbcAMP. *In vivo* grown control oocytes from 5 week old (C57BL × CBA) F1 females were obtained by puncturing isolated ovaries with hypodermic needles and then microinjected with mRNAs as described above.

In vitro fertilization

Oocytes grown for 10-11 days within follicles *in vitro* or obtained from adult (C57BL × CBA) F1 females (7-12 weeks old) were denuded and matured in follicle-culture medium (see above). MII oocytes were placed in 50 μl of EmbryoMax® HTF medium (Millipore) and fertilized with 10 μl of sperm suspension from 5-13 week old (C57BL × CBA) F1 males. The sperm suspension was prepared by dissecting two cauda epididymus from one male in 2 ml of HTF medium. After 4-6 h, zygotes were transferred to KSOM+AA (Millipore) and cultured for 5 days at 37°C.

Expression constructs and mRNA synthesis

To generate constructs for *in vitro* mRNA synthesis, the previously published protein coding sequences of *Mastl*[20] and α-tubulin[21] were fused with mEGFP and inserted into pGEMHE for *in vitro* transcription. The *Mus musculus Dusp7* ORF (derived from NM_153459) was amplified by PCR from mouse oocyte cDNA. The resulting product of around 1300 base pairs contained a 5′-XhoI and a 3′-EcoRI restriction site, which were used to insert it into pGEMHE-EGFP carboxyterminally of the EGFP tag. These constructs as well as pGEMHE-H2B-mRFP1[22], pGEMHE-EGFP-MAP4[22] and pGEMHE-EGFP-LaminB1[23] were linearised with AscI. Capped mRNA was synthesized using T7 polymerase (mMessage mMachine kit, following manufacturer's instructions, Ambion) and dissolved in 11 μl water. mRNA concentrations were determined on ethidium bromide agarose gels by comparison with an RNA standard (Ambion).

Confocal microscopy

Images were acquired with a Zeiss LSM710 confocal microscope equipped with a Zeiss environmental incubator box or a Zeiss LSM780 confocal microscope equipped with a Tokai Hit Stage Top Incubator, with a 40x C-Apochromat 1.2 NA water immersion objective lens for live oocytes, and a 63x C-Apochromat 1.2 NA water immersion objective for fixed oocytes as previously described[22]. In some images, shot noise was reduced with a Gaussian filter. Z-projections were generated in Zeiss' Zen software.

Measurement of chromosome volumes

Oocytes were fixed for 30 min at 37°C in 100 mM HEPES (pH 7) (titrated with KOH), 50 mM EGTA (pH 7) (titrated with KOH), 10 mM MgSO4, 2% formaldehyde (MeOH free) and 0.2% Triton X-100, based on previously published methods. DNA was stained with 0.05 μg/ml Hoechst 33342 (Molecular Probes). All stainings were performed in PBS, 0.1% Triton X-100, 3% BSA. Chromosome volumes were determined in 3D volume reconstructions using the surface function in Imaris (Bitplane).

siRNAs

All siRNAs were purchased from QIAGEN. siRNAs were diluted in 96-well plates to a concentration of 6.6 μM and stored at −80°C. To preselect genes, we took advantage of two microarray data sets[10,11], which compare the expression profile of oocytes with the profiles of other cell types and preimplantation mouse embryos, respectively. Only genes that were highly significantly upregulated in oocytes in both data sets were selected for the screen, independently of whether they had previously been implicated in mitosis or meiosis to avoid any bias. We targeted each gene with a low complexity siRNA pool (3 siRNAs per gene) (Supplementary Table 4), which on average leads to fewer off-target effects and higher penetrance of phenotypes than individual siRNAs[24,25]. For the primary RNAi screen, siRNAs targeting different genes were mixed and microinjected to a final concentration of 5 nM each in the oocyte. For the functional characterisation of individual genes, siRNA concentrations of up to 0.2 μM final in the oocyte were used. Protein ablation should always be assessed by secondary assays, because proteins that are generated in the very early stages of meiosis may still not be efficiently depleted if they do not turn over, even if the targeted transcript is reduced.

Quantitative real time PCR

mRNA was extracted using an RNeasy Mini Kit (Qiagen) and cDNA was generated using the High Capacity RNA-to-cDNA Kit (Applied Biosystems). Real-time PCR was performed with the 7900 HT Real-Time Fast PCR System (Applied Biosystems) using SYBR Green. *GAPDH* mRNA was used for normalization.

RNA sequencing

Total RNA was isolated using NucleoSpin® RNA XS (Macherey-Nagel) from *in vitro* grown oocytes after 10 days of follicle culture or from oocytes obtained directly from adult (C57BL × CBA) F1 females (7-11 weeks old). A total of 50 oocytes with an intact nucleus per sample were used and 3 samples per group were collected. RNA was extracted using NucleoSpin RNA XS (Macherey-Nagel). A cDNA library was prepared using SMARTer® Ultra™Low Input RNA for Sequencing (Clonetech Laboratories) and the samples were processed by BGI Tech Solutions. The cDNA product was synthesized and amplified using SMARTer PCR cDNA Synthesis Kit (Clontech) from the total RNA (10 ng) of sample. The cDNA was fragment by Covaris E210 (Covaris) and the median insert length was about 200bp. The paired-end cDNA library was prepared in accordance with Illumina's protocols with an insert size of 200 bp and sequenced for 100 bp by HiSeq2000 (Illumina).

Expression analysis

NOISeq: RNA-Seq based measurements of transcript abundances at the level of genes were represented by FPKMs (Fragments Per Kilobase of transcript per Million fragments mapped). FPKM is conceptually similar to the reads per kilobase per million reads sequenced (RPKM) measure, but it is easily adaptable for sequencing data from one to higher numbers of reads from single source molecules. In order to identify significantly differentially expressed genes *between in vitro* and *in vivo* grown oocytes, we used a non-parametric method encoded in NOISeq. For this purpose we first filtered for low count or

abundance using the “CPM” low count filter of NOISeq. This yielded a reduction from the original 16,343 genes to 11,470 genes. Significant differential expression between oocytes grown *in vivo* and *in vitro* was determined using NOISeq with the following parameters: (1) “tmm”, Trimmed Mean of log2 FPKM, normalization. (2) Biological replicates data and (3) Probability of differential expression q being set to 0.8 or above and log2 values being greater than or equal -1 or 1 for upregulated and downregulated genes respectively in the *in vitro* group. This yielded 146 up- and 67 downregulated genes in *in vitro* grown oocytes. The vast majority of genes (11,110) was unchanged between the two conditions.

DESeq2: RNA-Seq counts were considered with two “conditions” i.e. *in vivo* and *in vitro* with three replicates. The standard protocol for DESeq2 differential expression analyses was followed with default settings. We deemed genes to be up- or downregulated if log2 values were greater than or equal -1 or 1 for up- and downregulated genes respectively in *in vitro* group with false discovery rate (FDR or padj of DESEq2) less than 0.01 or 1%. We considered a particularly low value of false discovery rate because of overall low expression levels for transcripts. Hence, we used a more stringent FDR value. This yielded 282 up- and 163 genes downregulated *in vitro*.

Statistics

Average (mean), s.d. (standard deviation) and statistical significance based on Student’s t–test or Fisher’s exact test (two-tailed) were calculated in Microsoft Excel, assuming normal distribution and similar variance. No statistical methods were used to predetermine sample size. All error bars show standard deviation. All box plots show median (line), mean (small square), 5th, 95th (whiskers) and 25th and 75th percentile (boxes). Z-scores were calculated as the deviation of the mean of a single siRNA mix to the mean of all controls of the RNAi screen, normalized to the standard deviation of all controls. siRNA mixes were sorted according to their z-score. The dashed line in Fig. 2 and Extended Data Fig. 4 delineates mixes with a z-score higher than two standard deviations above the average value of all controls.

Data analysis

Phenotypes were evaluated manually by browsing the data in Zeiss’ Zen software. Defects and measurements (time points and spindle parameters) were then recorded on a home-made user interface in OriginPro 8.0 and processed in Microsoft Excel. Averages, standard deviation and statistical significance were calculated in Excel. Z scores were calculated as the deviation of the mean of a single mix to the overall mean of all controls, normalized to the standard deviation of all controls. Oocytes that died during imaging were not analysed and do not contribute to data set.

For Fig. 4c, we analysed data from all 2,241 oocytes, because lagging chromosomes are not very common in control oocytes, but likely to be triggered by various defects such as those induced by RNAi in the screen.

For the Jaccard index heatmap in Extended Data Fig. 9, RNAi screen phenotypes from both mix and control experiments were collected and wherever there were numerical values they

were converted appropriately into “yes” and “no” values based on mean and standard deviation of the distribution of numerical values. Further, “yes” values were categorized into “+” and “−“ groups based on whether a numerical entry was greater than (mean + standard deviation) or whether it was smaller than (mean − standard deviation). This information was converted to a network representation such that there are two types of nodes in the network oocytes and phenotypes (Extended Data Figure 9c An edge was made between oocyte and phenotype if a given oocyte scored “yes” for a given phenotype. This yielded a network that we termed Phenotype-Oocyte network, which included 5,203 edges (or associations) between 53 phenotypes and 1,504 oocytes. The distribution of the number of oocytes against the number of distinct phenotypes scored in them suggested that over 75% of oocytes, namely 1,195, have two or more phenotypes scored, suggesting that there were widespread multiple phenotypes scored for in the vast majority of oocytes, as expected. Hence, we sought to estimate the extent of co-occurring phenotypes across oocytes as a first step towards phenotype correlations. We calculated the Jaccard index between all possible pairs of phenotypes in the Phenotype-Oocyte network. The Jaccard index between phenotype i and phenotype j was defined as

$$\frac{[(\mathbf{Oocytes\ exhibiting\ Phenotype\ i}) \cap (\mathbf{Oocytes\ exhibiting\ Phenotype\ j})]}{[(\mathbf{Oocytes\ exhibiting\ Phenotype\ i}) \cup (\mathbf{Oocytes\ exhibiting\ Phenotype\ j})]}$$

∩ denotes “intersection” between sets of oocytes with phenotypes i,j. ∪ denotes “union” between sets of oocytes with phenotypes i,j.

The above formula for the Jaccard index captures the fraction of co-occurrence of phenotypes i and j in oocytes over the total observed number of instances of phenotypes i or j. The numerator denotes the number of oocytes in which phenotypes i and j were observed, while the denominator indicates the total number of oocytes in which either phenotypes i or j have been observed. The values of a Jaccard index range between 0 and 1. Zero signifies poor co-occurrence while “1” signifies high co-occurrence. We calculated the Jaccard index for all possible pairs of phenotypes in the Phenotype-Oocyte network. Out of a possible 1,378 ($53C_2$), we could obtain 844 pairs that displayed a Jaccard index greater than zero. We then clustered the profile of the Jaccard index between phenotypes represented as a matrix or table. For this purpose, we used pheatmap (http://cran.r-project.org/web/packages/pheatmap/index.html) with “mean” clustering and “Pearson correlation” options. In this way, we obtained three major clusters of phenotype correlations.

Measurement of oocyte diameter, spindle length and spindle width

Oocyte diameter, spindle length and width in metaphase I and metaphase II were measured using the Measurement function in Zeiss’ Zen software. To accurately measure the oocyte diameter, measurements were always taken in the centre of the oocyte as determined by the maximum radius of the oocyte. Spindle length and width were only measured in oocytes in which the spindle was parallel to the confocal imaging plane.

Extended Data

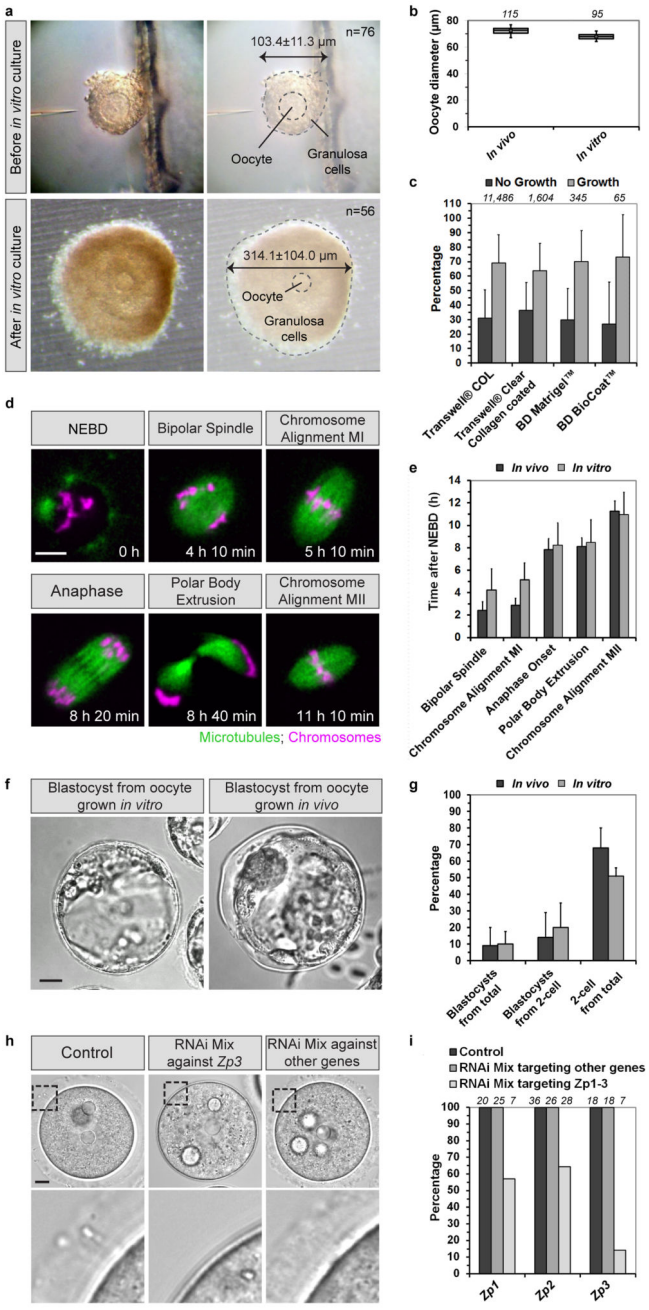

Extended Data Figure 1. Efficiency of follicle growth and comparison of *in vitro* and *in vivo* grown oocytes

(a) Follicles before (top panel) and after *in vitro* culture (bottom panel).The perimeter of oocyte and granulosa cells are highlighted on the right. The follicle diameter increases from 103.4±11.3 µm to 314.1±104.0 µm during *in vitro* culture. This lies between the diameter of *in vivo* grown early antral (~248 µm) and Graafian (~424 µm) mouse follicles[26], The diameter of *n* follicles was measured before and after *in vitro* culture and is displayed as

mean±s.d. Measurements from 3 or 2 independent experiments for before and after culture, respectively. **(b)** Diameter of *in vivo* or *in vitro* grown oocytes. Data from 2 and 7 experiments, respectively. The box plot shows median (line), mean (small square), 5th, 95th (whiskers) and 25th and 75th percentile (boxes). **(c)** Efficiency of follicle growth on different culture substrates. The number of independent experiments is 343, 56, 11 and 3 from left to right. The total number of follicles is specified in italics. Error bars show standard deviation. **(d)** Live oocyte expressing EGFP-MAP4 (green, microtubules) and H2B-mRFP (magenta, chromosomes). The characteristic time points of oocyte maturation that were determined for each oocyte in the screen (2,241 oocytes in total from 70 experiments) are listed above the representative images. Quantification of timing in (e). Scale bar, 10 μm. **(e)** The timing of bipolar spindle assembly, chromosome alignment during MI, anaphase, polar body extrusion and chromosome alignment during MII were quantified in oocytes obtained from five-week-old (C57BL × CBA) F1 females or in oocytes from the same strain grown *in vitro* within follicles. Data from 4 independent experiments. Error bars show standard deviation. **(f)** Transmitted light images of blastocysts derived from fertilized (C57BL × CBA) F1 oocytes grown *in vitro* within follicles (left) or *in vivo* (right)**.** Scale bar, 20 μm. Quantifications in (g). **(g)** (C57BL × CBA) F1 oocytes grown *in vitro* within follicles (left) or *in vivo* (right) were denuded, matured *in vitro*, and fertilised. The percentage of all oocytes (fertilised and unfertilised) that developed into 2-cell embryos (2-cell from total), and 2-cell embryos that developed into blastocysts (blastocyst from total) was quantified. Developmental rates are consistent with previous studies, in which *in vitro* matured denuded oocytes were fertilised[27,28], 179 *in vivo* grown and 180 *in vitro* grown oocytes were analysed in total. Data from 3 independent experiments for each group. Error bars show standard deviation. **(h)** Transmitted light images of control oocytes and oocytes microinjected with an siRNA mix targeting *Zp3* together with 11 other genes (RNAi Mix against *Zp3*) or an siRNA mix microinjected at the same time that targeted 12 other genes (RNAi mix against other genes). Highlighted region is magnified below. Scale bar: 10 μm. Quantification of phenotypes in (i). **(i)** The presence of the zona pellucida was scored in oocytes microinjected with control siRNA (Control), an siRNA mix targeting one of the three Zp genes (*Zp1*, *Zp2* or *Zp3*) together with 11 other genes and an siRNA mix microinjected at the same time that targeted 12 different genes (RNAi mix against other genes). The number of analysed oocytes is specified in italics.

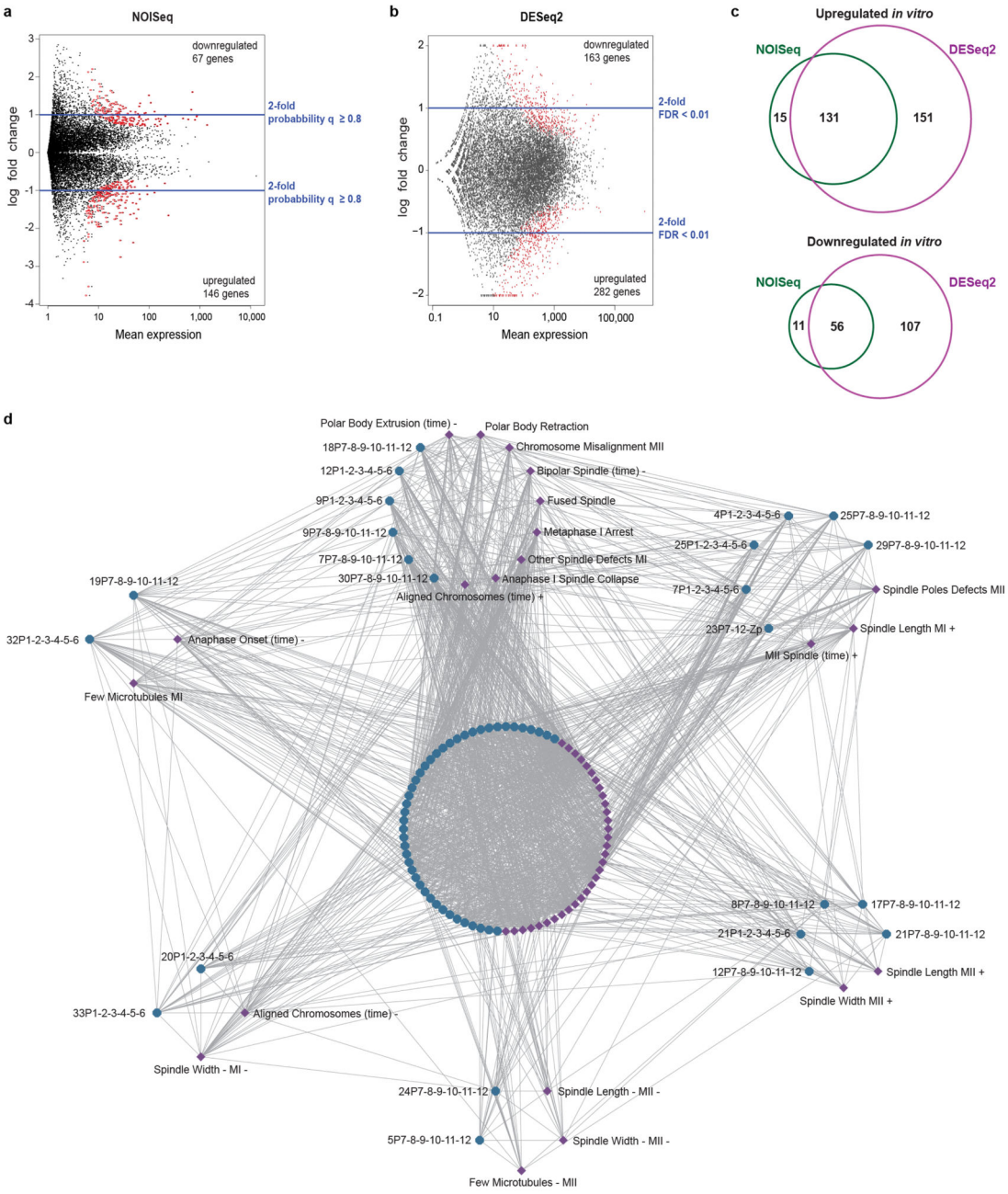

Extended Data Figure 2. Transcriptome analysis of *in vivo* and *in vitro* grown oocytes

(a-c) Transcriptome analysis of *in vitro* and *in vivo* grown oocytes. (a) Differentially expressed genes in oocytes grown *in vitro* based on evaluation using NOISeq algorithm. Transcript abundances are reported in transcript Fragments Per Kilobase per Million fragments mapped (FPKM). Only about 2% (213 out of 11,470) of genes were differentially expressed. (b) Differentially expressed genes in oocytes cultured *in vitro* based on evaluation using DESeq2 algorithm. Only about 4% (445 genes out of 10,597) of genes were differentially expressed after applying filters in both (b) and (c). The blue lines indicate

Europe PMC Funders Author Manuscripts

genes with at least 2-fold change in expression. Red colour indicates differentially expressed genes with the denoted probability. For details, please see Methods section. (c). The overlap between NOISeq and DESeq2 results, presented as Venn diagrams. There is at least over 80% overlap in genes in either up- or downregulated groups for both NOISeq and DESeq2. **(d)** Qualitative network of phenotypes in oocytes microinjected with siRNA mixes. Blue nodes represent siRNA mixes, purple nodes represent phenotypes. Grey lines between mixes and phenotypes denote if at least one oocyte microinjected with a given mix displayed the phenotype. The clusters indicate close relationship between a set of phenotypes and mixes. The clusters were obtained using ClusterViz (https://code.google.com/p/clusterviz-cytoscape/) of Cytoscape, which encodes the MCODE method to identify clusters of closed related nodes based on the topology of the network. The network contains 6 clusters identified by ClusterViz.

Europe PMC Funders Author Manuscripts

a

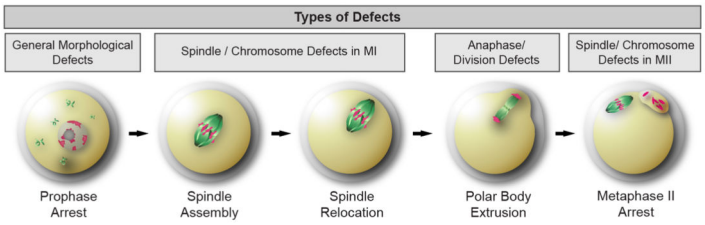

b

Type of Defect	Defect	Description of Defect
General Morphological Defects	More Pigment Granules	Pigment granules were defined as dark spots within the oocyte's cytoplasm and qualitatively analysed before nuclear envelope breakdown.
	Pigment Granules only at Cortex	
	Pigment Granules only in Centre	
	Static Cytoplasm	Assessed by qualitatively analysing pigment granule movement within the cytoplasm before nuclear envelope breakdown.
	Eccentric Nucleus	Nuclei were only classified as eccentric if they were positioned within 10 µm from the cortex
	Non-surrounded Nucleolar Chromatin Configuration	Oocytes without a perinucleolar heterochromatin rim
	No Nuclear Envelope Breakdown	Oocytes that stayed arrested in prophase for at least 18 hours after release from prophase arrest
Spindle Defects in Metaphase I and Metaphase II	No Spindle	Oocytes in which the spindle was absent
	Few Microtubules	Oocytes in which the number of microtubles was reduced
	No Ball Stage	Oocytes that directly formed a bipolar spindle after nuclear envelope breakdown or failed to form a proper microtubule ball with the chromosomes arranged on the ball's surface
	Arrest in Ball Stage	Oocytes that showed a microtubule ball with chromosomes arranged in a belt-like structure for at least 18 hours after nuclear envelope breakdown
	Spindle Pole Defects	Comprises multi- and monopolar spindles, and spindles with altered spindle pole morphology
	- Multipolar Spindle	Spindles with more than two focussed poles
	- Monopolar Spindle	Spindles with only one focussed pole
	- Altered Spindle Pole Morphology	Broad or hyperfocussed spindle poles
	Spindle Relocation Defect (only MI)	MI spindles that stayed in the centre of the oocyte until anaphase
	Spindle Collapse (only MI)	MI spindle microtubules that completely depolymerized before anaphase, sometimes reforming a spindle, sometimes not
	Other Spindle Defects (only MI)	Altered MI spindles which could not be classified in any of the above categories
Chromosome Defects in Metaphase I and Metaphase II	Chromosome Aggregates	Chromosomes that failed to separate
	Chromosome Stretching Defect	Chromosomes that were abnormally short
	Chromosome Misalignment	Chromosomes that were not aligned at the spindle equator
	Chromosome(s) Lost in Cytoplasm	Chromosomes that were unconnected to the spindle or separated from the majority of chromosomes if a spindle was missing
Anaphase Defects	Metaphase I Arrest	Oocytes that showed a bipolar spindle with aligned chromosomes and failed to progress into anaphase for at least 18 hours after nuclear envelope breakdown
	Lagging Chromosomes	Movement to spindle poles of some chromosomes during anaphase was slower than that of the majority of chromosomes
	Anaphase Spindle Collapse	MI spindle microtubules that completely depolymerized during polar body extrusion
Division Defects	Cytokinesis Defects	Comprises polar body retractions, symmetric division failures and unsuccessful cytokinesis
	- Polar Body Retraction	Half of the chromosomes were extruded in a protrusion resembling a polar body that subsequently retracted without cell division into polar body and egg
	- Symmetric Division Failure	Unsuccessful cytokinesis with furrow ingression in oocyte's centre
	Symmetric Division	Division into two cells of equal size
	Random Cortical Contractions	Simultaneous ingression of multiple furrows around the cortex during polar body extrusion
	Joined Spindle (only MII)	Following chromosome segregation in anaphase, chromosomes fuse again and arrange in a joined spindle

c

Type of Numerical Value	Numerical Value	Description of Numerical Value
Meiotic Time Points	Nuclear Envelope Breakdown	Time of nuclear envelope breakdown as evident from disappearance of nucleolus
	Bipolar Spindle Formation	First time a clear spindle axis is visible
	Chromosome Alignment	First time chromosomes congressed in metaphase plate
	Anaphase Onset	Onset of chromosome segregation
	Polar Body Extrusion	Time a polar body becomes visible
	MII Spindle Assembly	Time when a bipolar metaphase II spindle has assembled
Spindle Parameters	Spindle length (MI/MII)	Longest distance between the two spindle poles
	Spindle width (MI/MII)	Diameter of spindle in region of metaphase plate

Extended Data Figure 3. Description of defects scored in screen

(a) Scheme illustrating the main categories of defects that were quantified in the screen. **(b)** Table listing the main categories of defects and their subcategories as well as a description of each defect. **(c)** Table listing the numerical values that were measured in the screen and a description of each numerical value.

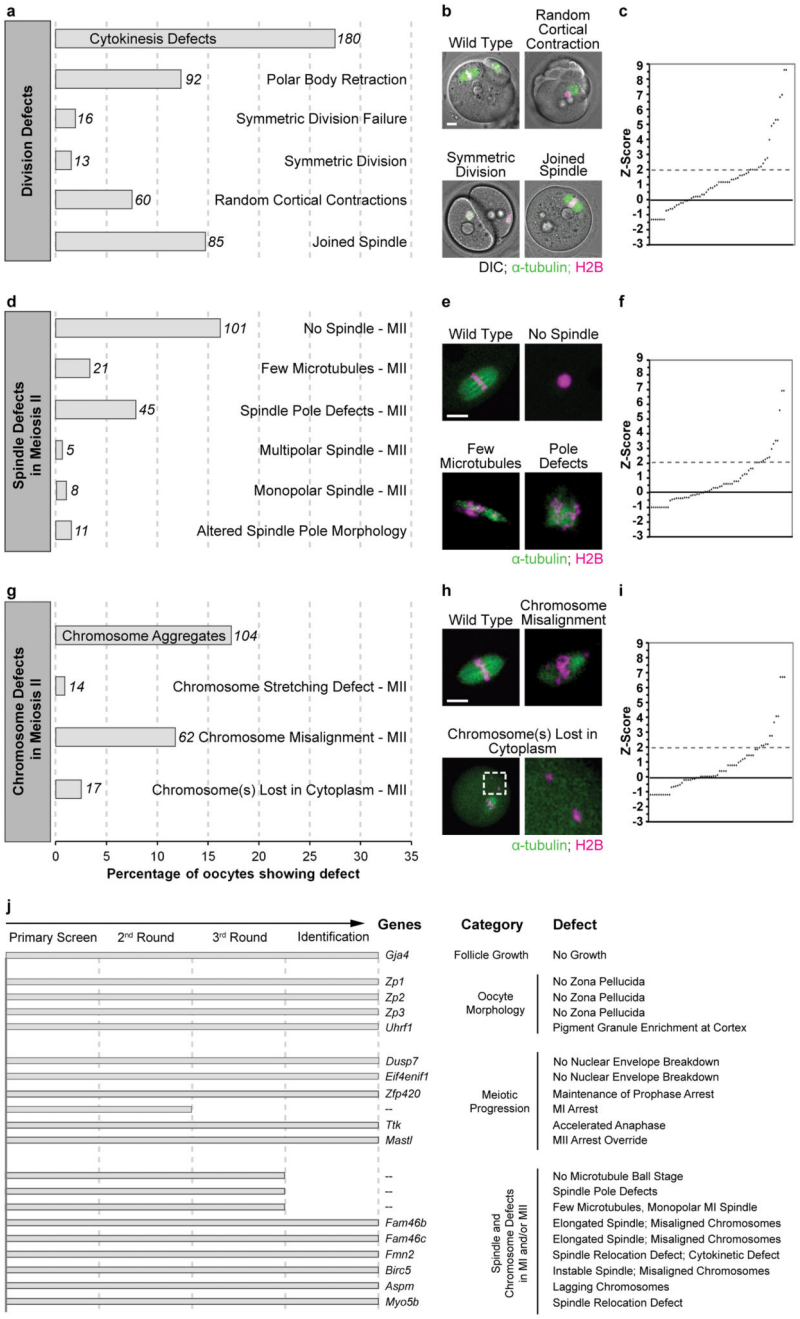

Extended Data Figure 4. Defects during meiosis II in siRNA-treated oocytes

(a,d,g) The frequency of cytokinetic defects (a), spindle defects in metaphase II (d), and chromosome defects in metaphase II **(g)** were scored in siRNA treated oocytes. The absolute number of oocytes with each defect is shown in italics. Data from 70 independent experiments. Corresponding control data are shown in Extended Data Fig. 5. **(b,e,h)** Examples of defects in live oocytes. Chromosomes (magenta) were labelled with H2B-mRFP, microtubules (green) with mEGFP-α-tubulin. Quantifications in (a,d,g). Scale bars: 10 μm. **(c,f,i)** z-scores we calculated as the deviation of the mean of a single siRNA mix to

the mean of all controls of the RNAi screen, normalized to the standard deviation of all controls. siRNA mixes were sorted according to their z-score. The dashed line delineates mixes with a z-score higher than two standard deviations above the average value of all controls. **(j)** List of genes that were tracked down to the individual gene level in RNAi screen. Please note that defects caused by depletion of some proteins such as *Zfp420* or *Uhrf1* may reflect the function of more proximal genes under the control of these proteins. We were able to allocate 16 out of 20 tested defects to individual genes. Defects that could not be tracked down to individual gene level are show as grey bars ending after the 2nd or 3rd round. S

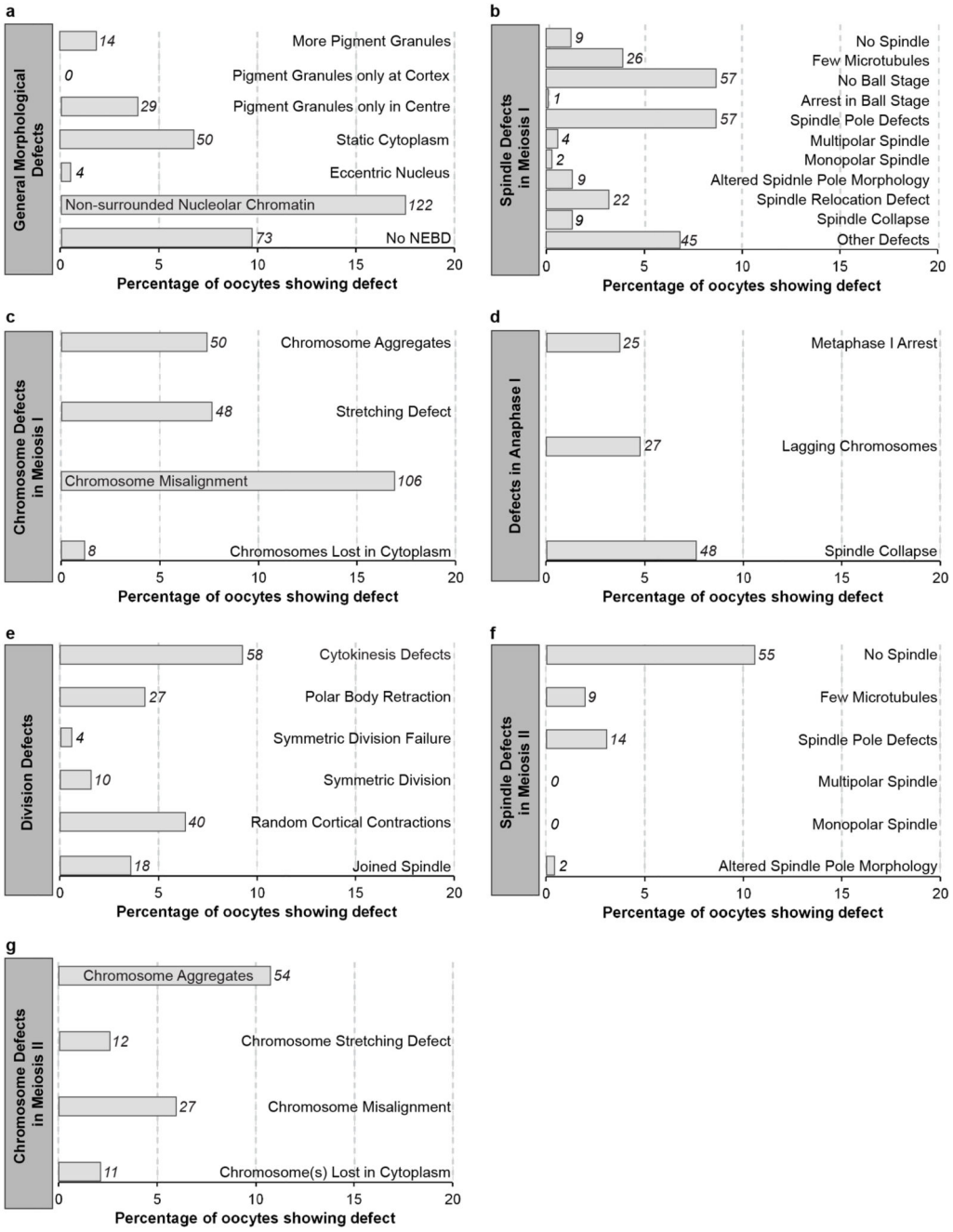

Extended Data Figure 5. Frequency of MI and MII defects in oocytes treated with control siRNAs

(a-g) The frequency of scored general morphological defects (NEBD – nuclear envelope breakdown) (a), spindle defects in MI (b), chromosome defects in MI (c), defects in anaphase I (d), defects during cytokinesis (e), spindle defects in MII (f) and chromosome defects in MII (g) were scored in oocytes microinjected with control siRNAs. The absolute number of oocytes with each defect is shown in italics.

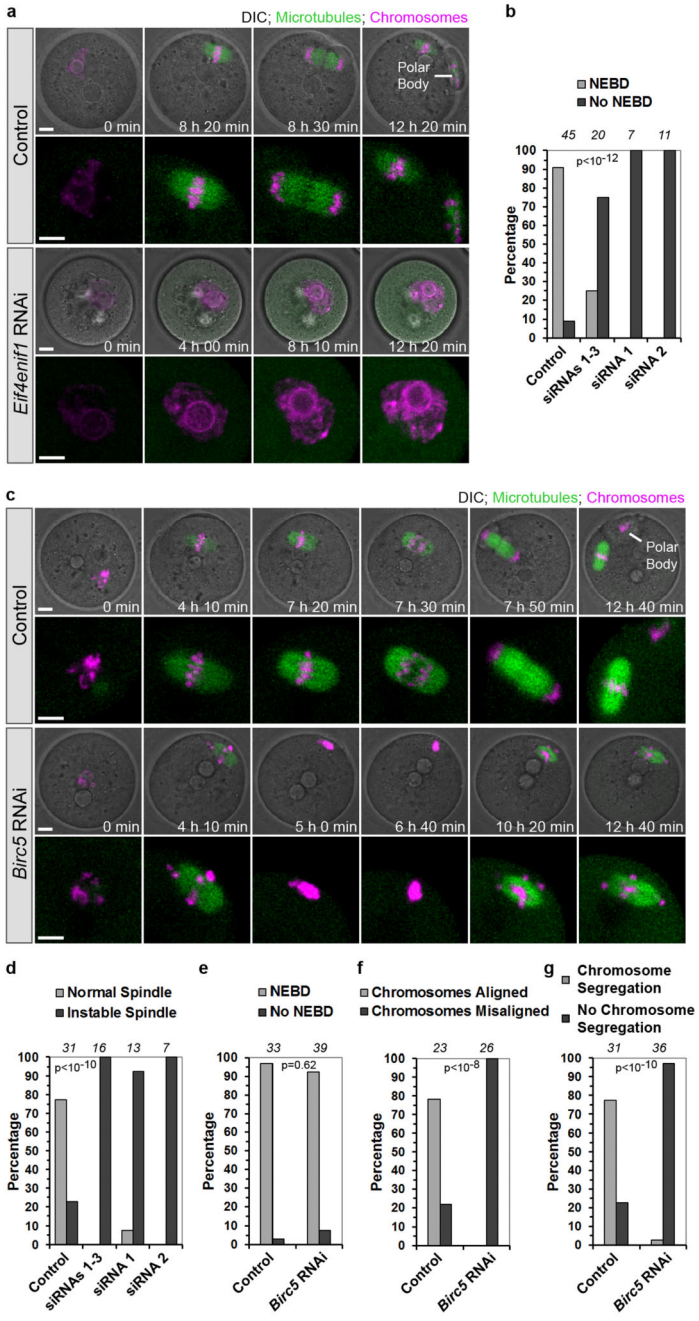

Extended Data Figure 6. *Eif4enif1* is required for release from prophase arrest and *Birc5* for spindle integrity

(a) Live oocytes microinjected with control siRNA (Control) or siRNAs targeting *Eif4enif1* (*Eif4enif1* RNAi) expressing mEGFP-α-tubulin (green, microtubules) and H2B-mRFP (magenta, chromosomes) merged with DIC. Region of spindle and chromosomes is magnified without DIC below. Quantification of phenotype in (b). Scale bar, 10 μm. **(b)** Live oocytes microinjected with control siRNA or *Eif4enif1* siRNAs were monitored by long-term time-lapse microscopy as shown in (a) and the efficiency of NEBD was scored. The number of analysed oocytes is specified in italics. P-value was calculated with Fisher's

Europe PMC Funders Author Manuscripts

exact test in Excel. Data from a total of 3 experiments. **(c)** Live oocytes microinjected with control siRNA (Control) or siRNAs targeting *Birc5* (*Birc5* RNAi) expressing mEGFP-α-tubulin (green, microtubules) and H2B-mRFP (magenta, chromosomes) merged with DIC. Region of spindle and chromosomes is magnified without DIC below. Quantification of phenotypes in (d-g). Scale bar, 10 μm. **(d)** Live oocytes microinjected with control siRNA (control), a mix of three different *Birc5* siRNAs (siRNA 1-3) or two *Birc5* siRNAs individually (siRNA 1,2) were scored for temporary or permanent disintegration of the meiotic spindle. The number of analysed oocytes is specified in italics. The P-value was calculated with Fisher's exact test comparing control and all *Birc5* siRNA microinjected oocytes from 5 experiments. **(e-g)** Live oocytes microinjected with control siRNA or *Birc5* siRNAs were monitored by long-term time-lapse microscopy as shown in (c) and the efficiency of NEBD (e), the presence or absence of misaligned chromosomes (f), as well as the efficiency of chromosome segregation (g) were scored. The number of analysed oocytes is specified in italics. P-values were calculated with Fisher's exact test in Excel. Data (d-g) from 5 independent experiments.

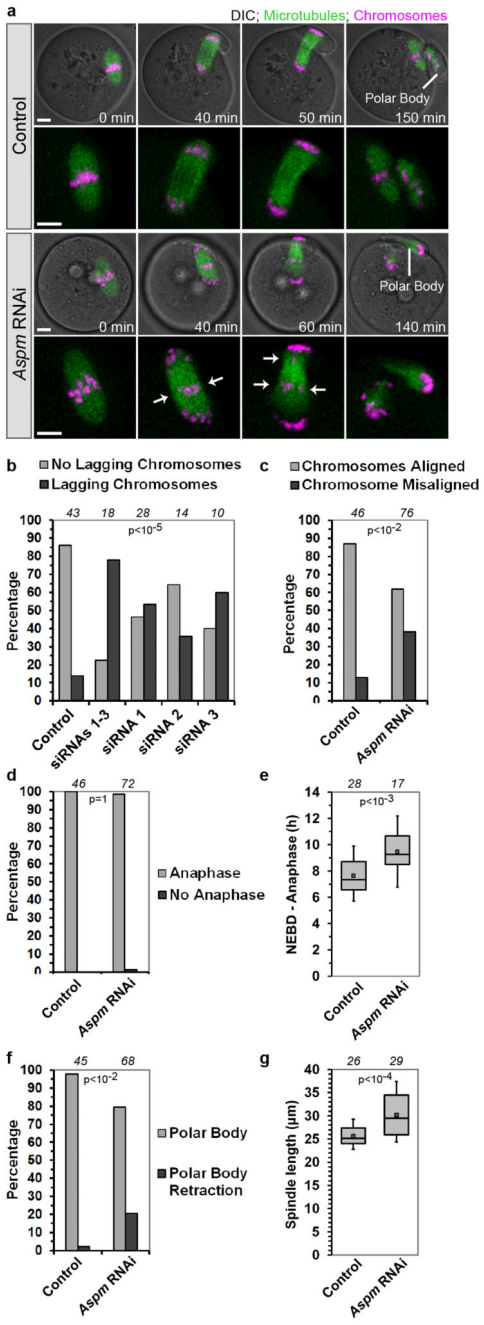

Extended Data Figure 7. *Aspm* function in mouse oocytes

(a) Oocytes microinjected with siRNAs targeting *Aspm* or injected with control siRNA. Microtubules in green, chromosomes in magenta. Arrows highlight lagging chromosomes. Quantification of phenotypes in (b-g). Scale bar, 10 µm. **(b,c)** Lagging (b) or misaligned chromosomes (c) in oocytes microinjected with different *Aspm* siRNAs. **(d-g)** Live oocytes microinjected with control siRNA (control) or *Aspm* siRNAs (*Aspm* RNAi) were monitored by long-term time-lapse microscopy as shown in (a) and scored for progression through anaphase (d), time of anaphase onset (e), polar body extrusion (f) and spindle length (g). The

number of analysed oocytes is specified in italics. The P-value was calculated with Fisher's exact test (b, c, d, f) or Student's t-test (e, g) comparing control and all *Aspm* siRNA microinjected oocytes. The box plots in (e, g) show median (line), mean (small square), 5th, 95th (whiskers) and 25th and 75th percentile (boxes). Data from 4 independent experiments.

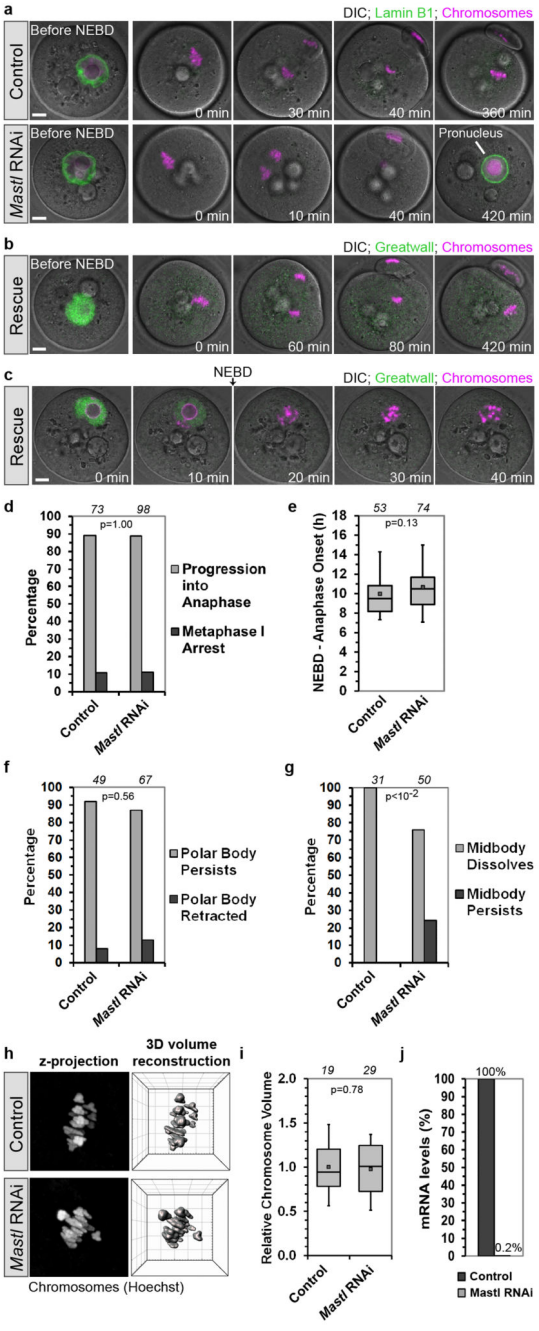

Extended Data Figure 8. *Mastl* is required for metaphase II arrest and accurate chromosome segregation, but dispensable for cytokinesis and chromosome condensation in mouse oocytes

(a) Live oocytes microinjected with control siRNA (Control) or siRNAs targeting *Mastl* (*Mastl* RNAi) expressing mEGFP-Lamin B1 (green, nuclear lamina) and H2B-mRFP

Europe PMC Funders Author Manuscripts

(magenta, chromosomes) merged with DIC. Representative of 30 control and 16 *Mastl* RNAi oocytes. Scale bar, 10 μm. **(b,c)** Live oocytes microinjected with a mix of three different *Mastl* siRNAs expressing human Greatwall fused with mEGFP (green) and H2B-mRFP (magenta, chromosomes) merged with DIC. EGFP-Gwl localized to the nucleus and was released into the cytoplasm shortly before NEBD. Representative of 23 oocytes. Quantification in Fig. 3f. (c), consistent with previous studies in mitotic cells [29,30]. Scale bar, 10 μm. **(d-g)** Live oocytes microinjected with control siRNA or *Mastl* siRNAs were monitored by long-term time-lapse microscopy and scored for anaphase progression (d), time of anaphase onset (e), successful formation or retraction of a polar body upon anaphase (f) and the prolonged presence of a midbody upon cytokinesis (g). The number of analysed oocytes is specified in italics. Data from 5 independent experiments **(h)** Maximum z-projection (left) and 3D reconstruction (right) of chromosomes (Hoechst) in fixed mouse oocytes microinjected with control siRNAs or siRNAs targeting *Mastl* were generated in Imaris. Quantification in (i). **(i)** The chromosome volume was quantified in mouse oocytes microinjected with control siRNAs or siRNAs targeting *Mastl* as shown in (h) in Imaris. The number of analysed oocytes is specified in italics. Data from 2 independent experiments. **(j)** *Mastl* mRNA levels in control oocytes and oocytes microinjected with *Mastl* siRNAs were quantified by real-time PCR. Mean values from two independent experiments. P-values were calculated with Fisher's exact test (d, f, g) or Student's t-test (e, i). The box plots in (e, j) show median (line), mean (small square), 5th, 95th (whiskers) and 25th and 75th percentile (boxes).

Europe PMC Funders Author Manuscripts

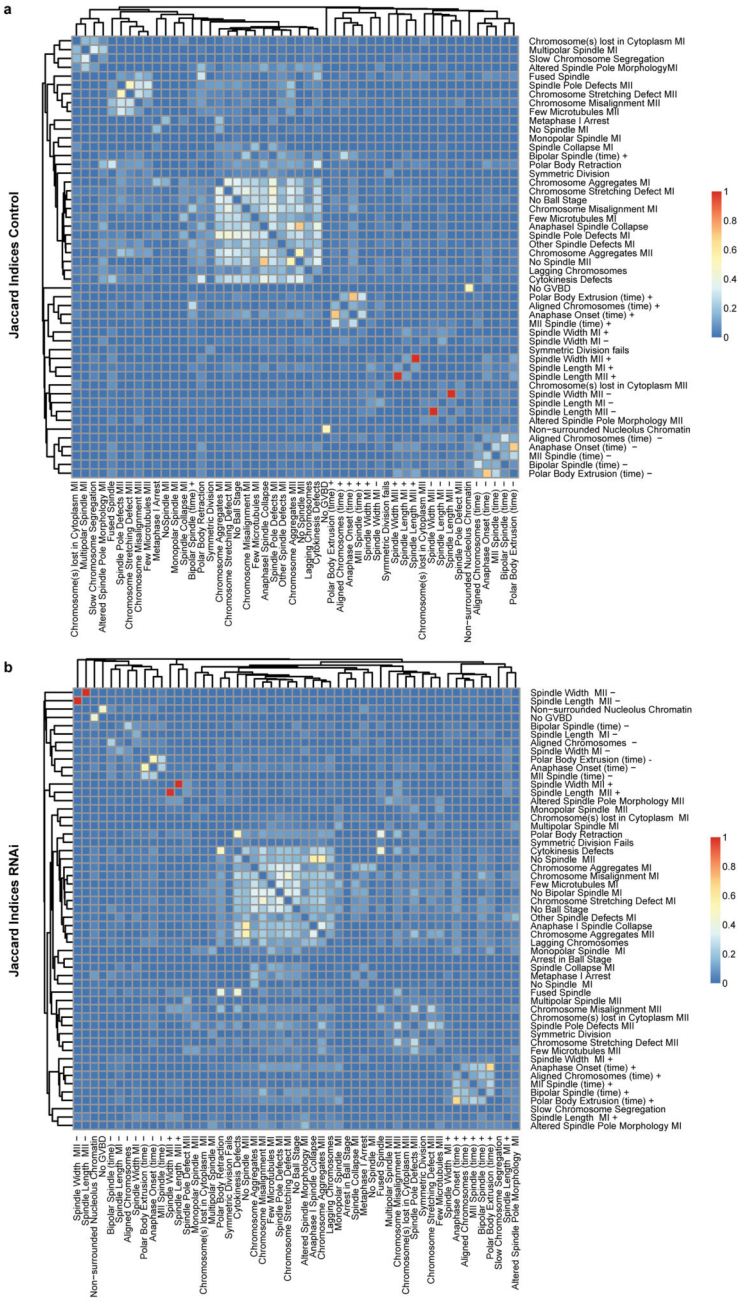

Extended Data Figure 9. Systematic analysis of phenotype correlations in mouse oocytes

(a.b) Heatmap representation of clusters of phenotypes generated based on Jaccard indices between them. Jaccard indices, range between 0 and 1, were calculated as described in Methods section and Extended Data Fig. 10. Jaccard indices calculated from control oocytes **(a)** and RNAi-treated oocytes **(b)** are shown. The “red” and “blue” respectively correspond to high and low Jaccard indices as indicated by the legend. Clusters of phenotypes were generated using Pheatmap with “Pearson correlation” values and “average” clustering input parameters.

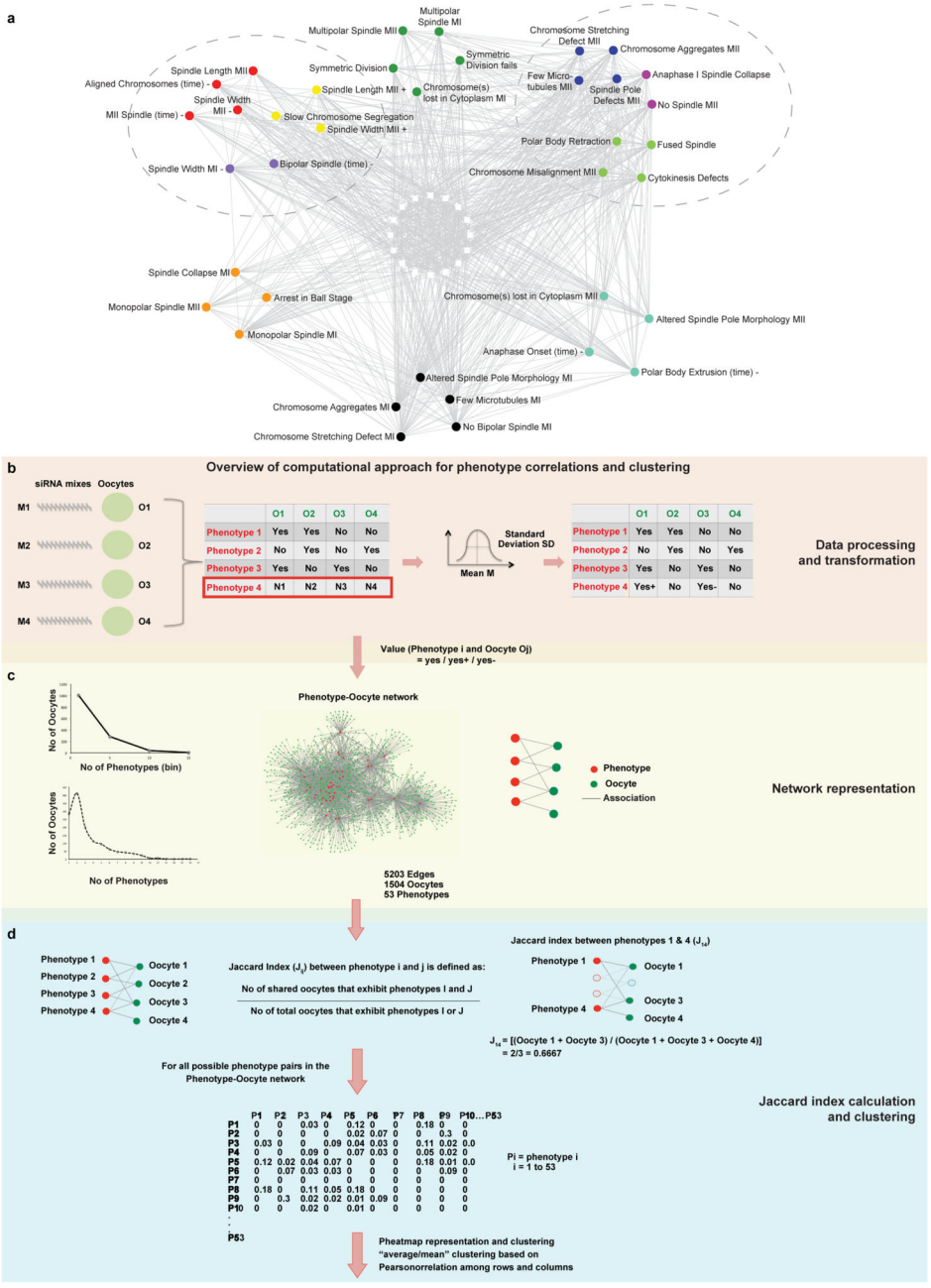

Extended Data Figure 10. Network of phenotypes and calculation of Jaccard indices

(a) Network of phenotype to oocytes was converted into phenotype-to-phenotype network based on number of oocytes that display two phenotypes in question. The network consists of 53 phenotypes and 867 connections between them. The nodes in the network denote phenotypes and edges denote shared oocytes. This is a qualitative network and does not consider the strength of connection, edge weight or number of oocytes in which a given pair of phenotypes co-occurs. Nodes of identical colours denote a cluster (a group of related phenotypes based on topological properties of the network). Phenotypes that are not part of

Europe PMC Funders Author Manuscripts

any cluster are in the centre and indicated by squares (white). Related clusters (if they share phenotypes) are marked by dashed circles considered as “super clusters”. Clusters were identified by the NeMo method in Cytoscape. Network clusters are purely based on topological properties and are in agreement with the clusters in the heatmap constructed using quantitative measures of Jaccard indices (Fig 9a) e.g. two superclusters: top left and top right respectively correspond to heatmap clusters at the top left and middle of Fig. 9a. (**b-d**) Overview of computational approach with schematics to decipher phenotype clusters. Oi, Mi and Ni correspond to oocyte i, mix i and numerical value of phenotype i, respectively. **(b)** Conversion of yes, no and numerical data: depicts the way we converted a combination of “yes”, “no” and numerical data (denoted by N1, N2, N3 and N4) of phenotypes across oocytes into purely “yes” and “no” groups with the “yes” group further classified as “yes+” and “yes−”. **(c)** Reconstruction of phenotype-oocyte network: we reconstructed a phenotype-oocyte network from the above data of “yes” and “no” values by considering only the “yes” group. A non-linear decay relationship between the number of phenotypes and number of oocytes in the network is displayed as represented by two plots. Details of the plots suggest a median value of 2 for phenotypes. **(d)** Network transformation and calculation of Jaccard index matrix: illustrates our network transformation strategy from a phenotype-oocyte network to a phenotype-phenotype network and the simultaneous estimation of Jaccard indices between phenotypes. The matrix of Jaccard indices between phenotypes was clustered using the pheatmap software in R package with the “Pearson correlation” parameter and the “average” clustering method.

Supplementary Material

Refer to Web version on PubMed Central for supplementary material.

Acknowledgements

The authors thank the staff of the LMB’s Animal and Microscopy Facilities for technical assistance; Jan Ellenberg, Laurinda Jaffe and Marina Freudzon for technical advice on culturing siRNA-injected follicles *in vitro*; Jan Ellenberg and M. Madan Babu for discussions; Guilhem Chalancon for help with data analyses; Eric Voets for the *Mastl* construct; and members of the Schuh lab and Sean Munro for comments on the manuscript. S.P. and M.P. received PhD fellowships from Boehringer-Ingelheim Fonds. T.T. is supported by an EMBO Long Term Fellowship (ALTF700-2014). The research leading to these results has received financial support from the European Research Council under grant agreement no. 337415 and the European Community’s Seventh Framework Programme (FP7/2007-2013) under grant agreement no. 241548.

REFERENCES

1. Kuliev A, Zlatopolsky Z, Kirillova I, Spivakova J, Cieslak Janzen J. Meiosis errors in over 20,000 oocytes studied in the practice of preimplantation aneuploidy testing. Reprod Biomed Onlinae. 2011; 22:2–8. doi:10.1016/j.rbmo.2010.08.014. [PubMed: 21115270]
2. Fragouli E, et al. The cytogenetics of polar bodies: insights into female meiosis and the diagnosis of aneuploidy. Mol Hum Reprod. 2011; 17:286–295. doi:DOI 10.1093/molehr/gar024. [PubMed: 21493685]
3. Brar GA, Amon A. Emerging roles for centromeres in meiosis I chromosome segregation. Nat Rev Genet. 2008; 9:899–910. doi:10.1038/nrg2454. [PubMed: 18981989]
4. Nagaoka SI, Hassold TJ, Hunt PA. Human aneuploidy: mechanisms and new insights into an age-old problem. Nat Rev Genet. 2012; 13:493–504. [PubMed: 22705668]
5. Jones KT, Lane SI. Molecular causes of aneuploidy in mammalian eggs. Development. 2013; 140:3719–3730. doi:10.1242/dev.090589. [PubMed: 23981655]

6. Clift D, Schuh M. Restarting life: fertilization and the transition from meiosis to mitosis. Nat Rev Mol Cell Biol. 2013; 14:549–562. doi:10.1038/nrm3643. [PubMed: 23942453]
7. Jaffe LA, Norris RP, Freudzon M, Ratzan WJ, Mehlmann LM. Microinjection of follicle-enclosed mouse oocytes. Methods Mol Biol. 2009; 518:157–173. doi:10.1007/978-1-59745-202-1_12. [PubMed: 19085139]
8. Eppig JJ, Schroeder AC. Capacity of mouse oocytes from preantral follicles to undergo embryogenesis and development to live young after growth, maturation, and fertilization in vitro. Biol Reprod. 1989; 41:268–276. [PubMed: 2508774]
9. Mehlmann LM. Oocyte-specific expression of Gpr3 is required for the maintenance of meiotic arrest in mouse oocytes. Dev Biol. 2005; 288:397–404. [PubMed: 16289135]
10. Su AI, et al. A gene atlas of the mouse and human protein-encoding transcriptomes. Proc Natl Acad Sci U S A. 2004; 101:6062–6067. doi:10.1073/pnas.0400782101 [pii]. [PubMed: 15075390]
11. Zeng F, Baldwin DA, Schultz RM. Transcript profiling during preimplantation mouse development. Dev Biol. 2004; 272:483–496. doi:10.1016/j.ydbio.2004.05.018S0012160604003628 [pii]. [PubMed: 15282163]
12. Bleil JD, Wassarman PM. Synthesis of zona pellucida proteins by denuded and follicle-enclosed mouse oocytes during culture in vitro. Proceedings of the National Academy of Sciences of the United States of America. 1980; 77:1029–1033. [PubMed: 6928658]
13. Kasippillai T, et al. Mutations in eIF4ENIF1 are associated with primary ovarian insufficiency. The Journal of clinical endocrinology and metabolism. 2013; 98:E1534–1539. doi:10.1210/jc.2013-1102. [PubMed: 23902945]
14. Xu XL, et al. The microtubule-associated protein ASPM regulates spindle assembly and meiotic progression in mouse oocytes. PLoS One. 2012; 7:e49303. doi:10.1371/journal.pone.0049303. [PubMed: 23152892]
15. Jiang ZZ, et al. Survivin is essential for fertile egg production and female fertility in mice. Cell Death Dis. 2014; 5 doi:Artn E1154 Doi 10.1038/Cddis.2014.126.
16. Hached K, et al. Mps1 at kinetochores is essential for female mouse meiosis I. Development. 2011; 138:2261–2271. doi:10.1242/dev.061317. [PubMed: 21558374]
17. Adhikari D, et al. Mastl is required for timely activation of APC/C in meiosis I and Cdk1 reactivation in meiosis II. Journal of Cell Biology. 2014; 206:843–853. doi:DOI 10.1083/jcb.201406033. [PubMed: 25246615]
18. Salmon ED, Cimini D, Cameron LA, DeLuca JG. Merotelic kinetochores in mammalian tissue cells. Philosophical transactions of the Royal Society of London. Series B, Biological sciences. 2005; 360:553–568. doi:10.1098/rstb.2004.1610. [PubMed: 15897180]
19. Cimini D. Merotelic kinetochore orientation, aneuploidy, and cancer. Biochim Biophys Acta. 2008; 1786:32–40. doi:10.1016/j.bbcan.2008.05.003. [PubMed: 18549824]

REFERENCES FOR METHODS AND EXTENDED DATA FIGURES

20. Voets E, Wolthuis RM. MASTL is the human orthologue of Greatwall kinase that facilitates mitotic entry, anaphase and cytokinesis. Cell Cycle. 2010; 9:3591–3601. [PubMed: 20818157]
21. Mora-Bermudez F, Gerlich D, Ellenberg J. Maximal chromosome compaction occurs by axial shortening in anaphase and depends on Aurora kinase. Nat Cell Biol. 2007; 9:822–831. doi:ncb1606 [pii]10.1038/ncb1606. [PubMed: 17558394]
22. Schuh M, Ellenberg J. Self-organization of MTOCs replaces centrosome function during acentrosomal spindle assembly in live mouse oocytes. Cell. 2007; 130:484–498. [PubMed: 17693257]
23. Lenart P, et al. Nuclear envelope breakdown in starfish oocytes proceeds by partial NPC disassembly followed by a rapidly spreading fenestration of nuclear membranes. J Cell Biol. 2003; 160:1055–1068. doi:10.1083/jcb.200211076. [PubMed: 12654902]
24. Echeverri CJ, Perrimon N. High-throughput RNAi screening in cultured cells: a user's guide. Nat Rev Genet. 2006; 7:373–384. doi:10.1038/nrg1836. [PubMed: 16607398]

25. Parsons BD, Schindler A, Evans DH, Foley E. A direct phenotypic comparison of siRNA pools and multiple individual duplexes in a functional assay. PLoS One. 2009; 4:e8471. doi:10.1371/journal.pone.0008471. [PubMed: 20041186]
26. Griffin J, Emery BR, Huang I, Peterson CM, Carrell DT. Comparative analysis of follicle morphology and oocyte diameter in four mammalian species (mouse, hamster, pig, and human). J Exp Clin Assist Reprod. 2006; 3:2. doi:10.1186/1743-1050-3-2. [PubMed: 16509981]
27. Ge L, et al. Factors affecting the in vitro action of cumulus cells on the maturing mouse oocytes. Molecular reproduction and development. 2008; 75:136–142. doi:10.1002/mrd.20753. [PubMed: 17440975]
28. Zhou P, et al. Mouse cumulus-denuded oocytes restore developmental capacity completely when matured with optimal supplementation of cysteamine, cystine, and cumulus cells. Biol Reprod. 2010; 82:759–768. doi:10.1095/biolreprod.109.082206. [PubMed: 20075397]
29. Alvarez-Fernandez M, et al. Greatwall is essential to prevent mitotic collapse after nuclear envelope breakdown in mammals. Proc Natl Acad Sci U S A. 2013; 110:17374–17379. doi:10.1073/pnas.1310745110. [PubMed: 24101512]
30. Wang P, et al. Cell cycle regulation of Greatwall kinase nuclear localization facilitates mitotic progression. J Cell Biol. 2013; 202:277–293. doi:10.1083/jcb.201211141. [PubMed: 23857770]

Europe PMC Funders Author Manuscripts

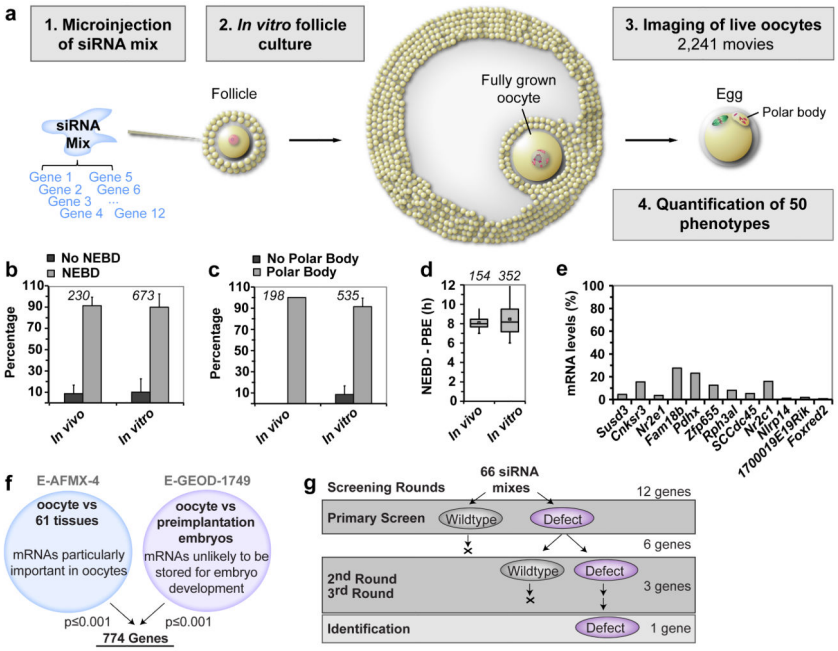

Figure 1. RNAi screen in live oocytes

(a) Principle of the screen. **(b-d)** Meiotic progression in oocytes grown *in vivo* (5 independent experiments) and *in vitro* (42 independent experiments). The box plot in (d) shows median (line), mean (small square), 5th, 95th (whiskers) and 25th and 75th percentile (boxes). **(e)** mRNA depletion upon targeting 12 genes simultaneously by RNAi. Representative example for 4 independent experiments. Errors bars in (b-d) show standard deviation.

(f) Selection of target genes. **(g)** Strategy to identify genes in mixes causing phenotypes.

Europe PMC Funders Author Manuscripts

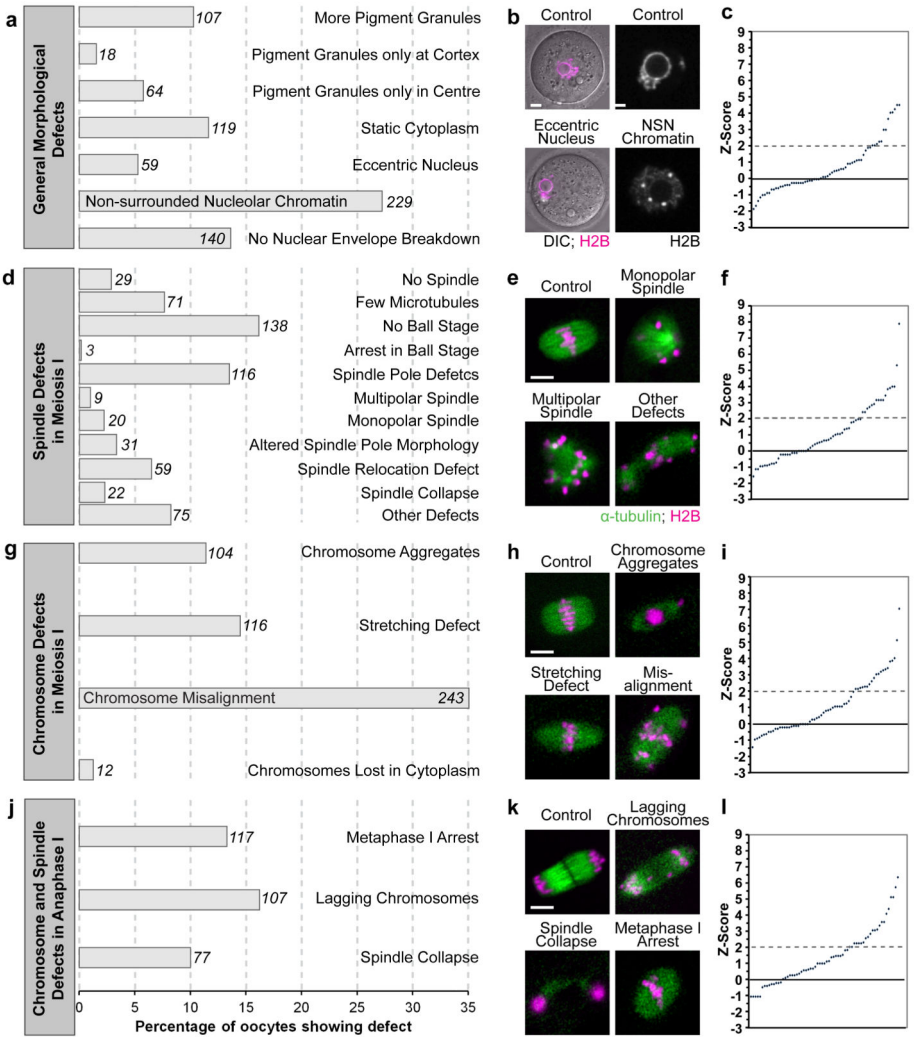

Figure 2. Defects during meiosis I in siRNA-treated oocytes

(a,d,g,j) Frequency of defects in siRNA-treated oocytes. Number of oocytes in italics. 70 independent experiments.

(b,e,h,k) Representative examples of phenotypes quantified in (a, d, g, j). Chromosomes (magenta; white in (b)), microtubules (green). NSN - non-surrounded nucleolus chromatin configuration. Scale bar, 10 μm.

(c,f,i,l) siRNA mixes sorted according to z-score in each category. Dashed line delineates mixes with a z-score higher than two standard deviations above the average value of all controls.

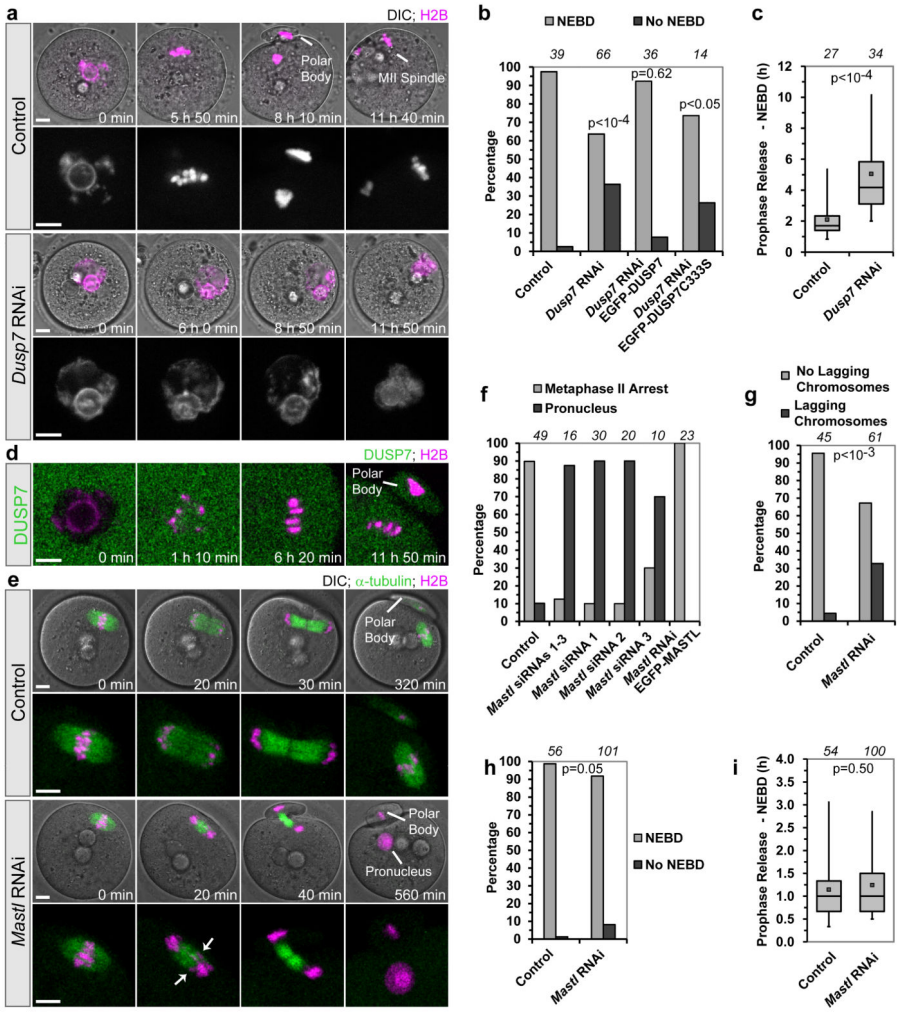

Figure 3. *Dusp7* and *Mastl* depletion phenotypes

(a) Oocytes microinjected with control or *Dusp7* siRNAs. Chromosomes in magenta. Quantification of phenotype in (b, c). Scale bar, 10 μm.

(b,c) Efficiency (b) and timing of NEBD (c) in oocytes microinjected with *Dusp7* siRNAs alone or together with mRNA encoding EGFP-DUSP7 or EGFP-DUSP7 C333S.

(d) Localization of DUSP7 during oocyte maturation. Live oocytes expressing DUSP7 fused with mEGFP (green) and H2B-mRFP (magenta, chromosomes). Scale bar, 10 μm. Representative for 36 oocytes from 5 experiments.

(e) Oocytes microinjected with control or *Mastl* siRNAs. Microtubules in green, chromosomes in magenta. Arrows highlight lagging chromosomes. Quantification of phenotypes in (f-i). Scale bar, 10 μm.

(f-i) Oocytes microinjected with different *Mastl* siRNAs alone or together with mRNA encoding human EGFP-MASTL were scored for formation of pronuclei (f), lagging chromosomes (g), and efficiency (h) and timing of NEBD (i).

Number of oocytes in italics. P-values were calculated with Fisher's exact (b, g, h) or Student's t-test (c, i). Data from 6 (b, c), 2 (f) or 5 (g, h, i) independent experiments. The

box plots in (c, i) show median (line), mean (small square), 5th, 95th (whiskers) and 25th and 75th percentile (boxes).

Europe PMC Funders Author Manuscripts

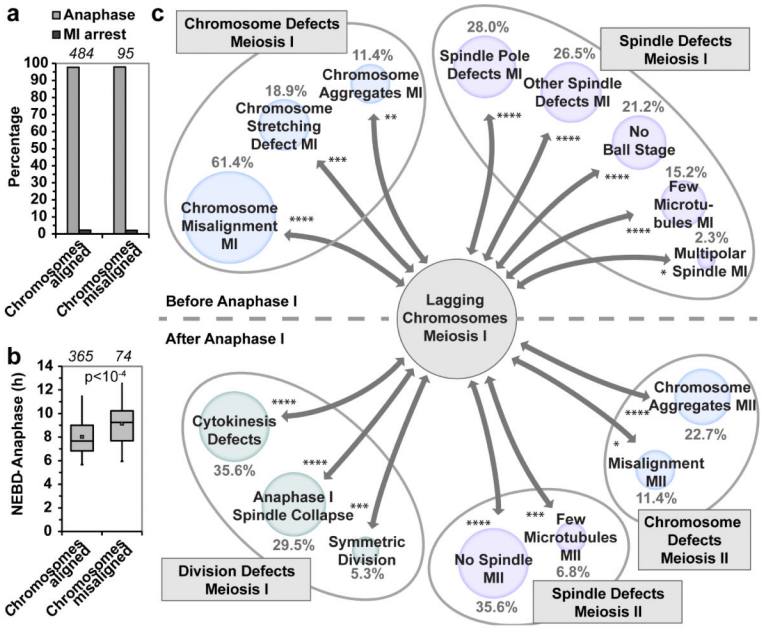

Figure 4. Factors implicated in chromosome segregation errors

(a,b) The efficiency (a) and timing (b) of progression into anaphase in control oocytes with aligned and misaligned chromosomes. Number of oocytes in italics. P-value was calculated with Fisher's exact test. Data from 52 independent experiments. **(c)** Defects significantly more likely to occur in oocytes with lagging chromosomes. Significance was calculated with Fisher's exact test by comparing the prevalence of other defects in oocytes with and without lagging chromosomes, and is specified by asterisks next to arrows, with **** $p < 0.0001$; *** $p < 0.001$; ** $p < 0.01$; * $p < 0.05$. The circle area reflects the fraction of oocytes with lagging chromosomes (specified in percent) in which each defect was observed.

Europe PMC Funders Author Manuscripts